AN EVALUATION OF AN EMPIRICAL MODEL FOR STALL DELAY DUE TO ROTATION FOR HAWTS

James L. Tangler
National Renewable Energy Laboratory
1617 Cole Boulevard
Golden, CO 80401

Michael S. Selig
Department of Aeronautical and Astronautical Engineering
University of Illinois at Urbana-Champaign
306 Talbot Laboratory, 104 South Wright Street
Urbana, IL 60801-2935

ABSTRACT

The objective of this study was to evaluate the Corrigan and Schillings stall delay model for predicting rotor performance for horizontal axis wind turbines. Two-dimensional (2D) wind tunnel characteristics with and without stall delay were used in the computer program PROP93 to predict performance for the NREL Combined Experiment Rotor (CER) and a lower solidity commercial machine. For the CER, predictions were made with a constant-chord/twisted blade and a hypothetical tapered/twisted blade. Results for the constant-chord/twisted blade were compared with CER data. Predicted performance using this empirical stall-delay method provided significant increases in peak power over 2D post-stall airfoil characteristics. The predicted peak power increase due to stall delay for the CER was found to be quite large (20% to 30%) as a result of its high blade solidity. For a more typical, lower-solidity commercial blade the predicted peak power increase was 15% to 20%. As described in the paper, correlation with test data was problematic due to factors not related to the stall-delay model.

INTRODUCTION

The accuracy of blade-element/momentum performance prediction codes such as PROP93 is dependent on the input airfoil characteristics, namely, the lift coefficient (c_l) and drag coefficient (c_d). These airfoil characteristics are typically based on two-dimensional (2D) wind-tunnel measurements that are known to normally underpredict peak power by 10% to 30% as well as the associated blade flapwise bending moment. Experimentally measured airfoil characteristics on rotating blades have found them to be substantially altered over the inboard portion of the blade by three-dimensional (3D) effects due to rotation.[1-5] These effects result in airfoil maximum lift coefficients ($c_{l,max}$) much larger than 2D measurements. The increase in $c_{l,max}$ has been attributed to centrifugal pumping which is modified by a Coriolis displacement in the chordwise direction.[6] Blade rotation results in centrifugal-induced outward radial flow in the separated flow region. The radial flow due to rotation develops in the presence of an adverse velocity gradient where the flow is strongly retarded. These effects have been modeled with complex computational fluid dynamics (CFD) methods.[7,8] For design purposes, simplified empirical methods are needed that capture the first-order effects due to rotation.

Three noteworthy empirical methods with a common basis have provided qualitative predictions and in some cases shown good agreement with experimental results. These methods provide approximations for radial flow modified by a Coriolis displacement that results in stall delay. The radial flow has been found to result from centrifugal force and the radial pressure gradient. Analytical considerations have shown the centrifugal component to be a function of the ratio of local chord to local radius (c/r). The radial pressure gradient has been more difficult to quantify. Eggers and Digumarthi[9] developed an approximate model to calculate the effects

Presented at the WINDPOWER '97 Conference
Austin, Texas, June 15-18, 1997

resulting from centrifugal viscous pumping and the resulting Coriolis displacement associated with deep-stalled flow. Their method relies on 2D wind-tunnel pressure data to calculate inplane and out-of-plane increments that are added to the 2D results. Predictions with this method for the constant-chord, non-twisted Combined Experiment Rotor (CER) blades showed good agreement with power measurements. Corrigan and Schillings[4] developed a simple method that calculates a stall delay angle for use in modifying the 2D wind-tunnel data. This method accounts for both centrifugal and radial pressure gradient effects and has been used successfully for helicopter rotors and prop-rotors to better predict stall delay effects on rotor loads and performance for high-thrust conditions. Recent work by Snel et al.[5] also recognized the dependency of stall delay on the blade shape parameter c/r associated with centrifugal/Coriolis effects and the radial pressure gradient. Their results also show a promising basis for predicting the 3D effects due to blade rotation.

The method of Corrigan and Schillings[4] was chosen for this evaluation because of it's simplicity and ability to quantify the influence of centrifugal force and the radial pressure gradient by calculating a stall-delay angle. The stall-delay angle is then used to adjust 2D airfoil data of c_l and c_d which results in greater c_l and a lower c_d. The modified airfoil data can then be used in PROP93 to predict enhanced peak power as a result of blade rotation. Providing that the method of Corrigan and Schillings yields realistic results for wind turbines, designers would then be able to better predict peak power and the associated blade loads.

EMPIRICAL STALL DELAY MODEL

The method of Corrigan and Schillings[4] and others[5,9] is based on a shape function or local solidity which relates the stall delay to the ratio of the local blade chord divided by its radial distance (c/r) from the center of rotation as shown in Fig.1. This representation implies that the centrifugal induced outward flow coupled with a Coriolis displacement is proportional to the ratio of the local c/r and that stall delay increases with local blade solidity. Radial flow reduces the suction surface boundary-layer thickness, the resulting drag, and the associated decambering of the airfoil. The calculations assume an external flow having a linear adverse velocity gradient over the airfoil's suction surface given by Equation 1.

$$u(z \rightarrow \infty) = \Omega r(1 - K\theta)\left[1 - K\left(\frac{c}{r}\right)\right] \tag{1.}$$

The separation point defined by $\partial u/\partial z = 0$, assumed to be at the trailing edge, was determined for a range of velocity gradient (K) values. The separation point is related to the velocity gradient K through the universal curve shown in Fig. 2.

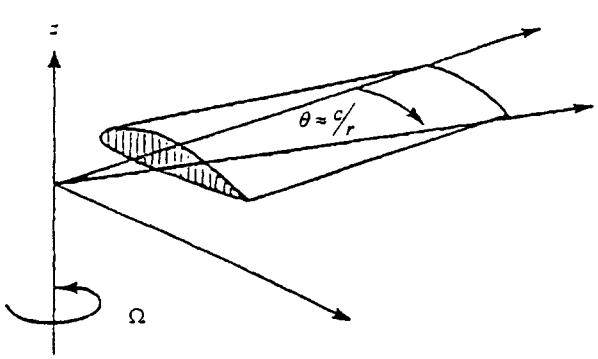

Fig. 1 Coordinate system used by Banks and Gadd (Ref. 6).

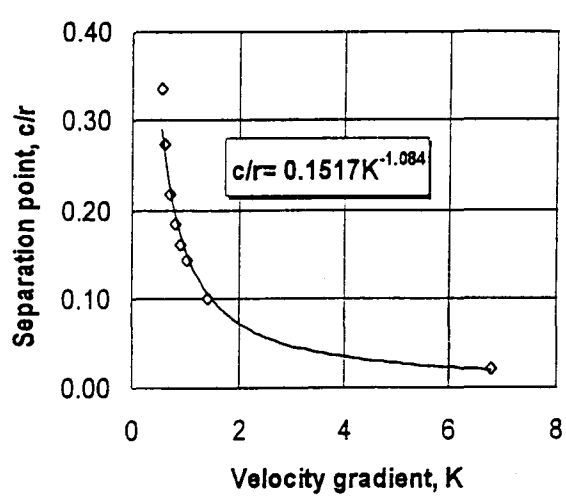

Fig. 2 Relationship for velocity gradient K and the separation point.

While partly based on analytical considerations,[6] the calculation for the stall-delay angle was largely derived through correlation with helicopter and prop-rotor test data over several years and is given by Equation 2.

$$\Delta\alpha = \left(\alpha_{C_{l,\max}} - \alpha_{C_{l=0}}\right)\left[\left(\frac{K\theta_{TE}}{0.136}\right)^{n} - 1\right] \tag{2.}$$

Equation (2) can be thought of as the product of an aerodynamic and centrifugal component. The aerodynamic component, the difference between the angle of attack at $c_{l,max}$ and the angle of attack at zero lift, implies that high $c_{l,max}$ airfoils result in a larger radial pressure gradient that contributes to the outboard radial flow which results in more stall delay than low $c_{l,max}$ airfoils. This empirical component was necessary to achieve correlation with helicopter and prop-rotor data sets. The centrifugal component is based on analytical considerations[6] from the momentum and continuity equations. This component relates to the local blade solidity and implies that greater local solidity and overall blade solidity results in more stall delay due to centrifugal pumping. The strength of the centrifugal term is proportional to the exponent n. For n=0, the stall delay becomes zero which is characteristic of 2D data. Corrigan[4] indicates that n varies from 0.8 to 1.6 to provide correlation with most test data and that n=1 provides good results for most cases. Based on this recommendation, n=1 was used throughout this evaluation.

APPLICATION TO STALL REGULATED TURBINES

The combined experiment rotor was chosen for verification of the stall delay model due to available test data related to this machine. This includes a 2D-airfoil data set for the machine's NREL S809 airfoil measured by Somers[10] in the Delft University of Technology low-speed wind tunnel. Rotor performance was predicted using PROP93[11] with 2D Delft data and with these data modified with the post-stall model. Calculations were done for the CER having constant-chord/twisted blades and a hypothetical tapered/twisted blade similar to one to be fabricated. Predicted results for the constant-chord/twisted blade were compared with measured CER data. Due to its high solidity and low rpm, the CER was not characteristic of most commercial machines. Therefore, the low solidity AWT-26 rotor was also chosen for analysis and comparison with available test data.

CER Rotor Model

The three-bladed CER models used in PROP93 consist of ten radial segments per blade with a root cutout of 20% as seen in Fig. 3. The twist distribution is exponential with most of the twist toward the root. An equivalent tapered planform with the same chord at 80% radius results in a similar peak power as the constant chord blade. Using the Corrigan and Schillings equation, stall delay was calculated from root to tip for the constant chord and tapered planform as shown in Table 1. Relative to the constant chord blade, the tapered blade has a greater amount of stall delay toward the blade root and less toward the blade tip.

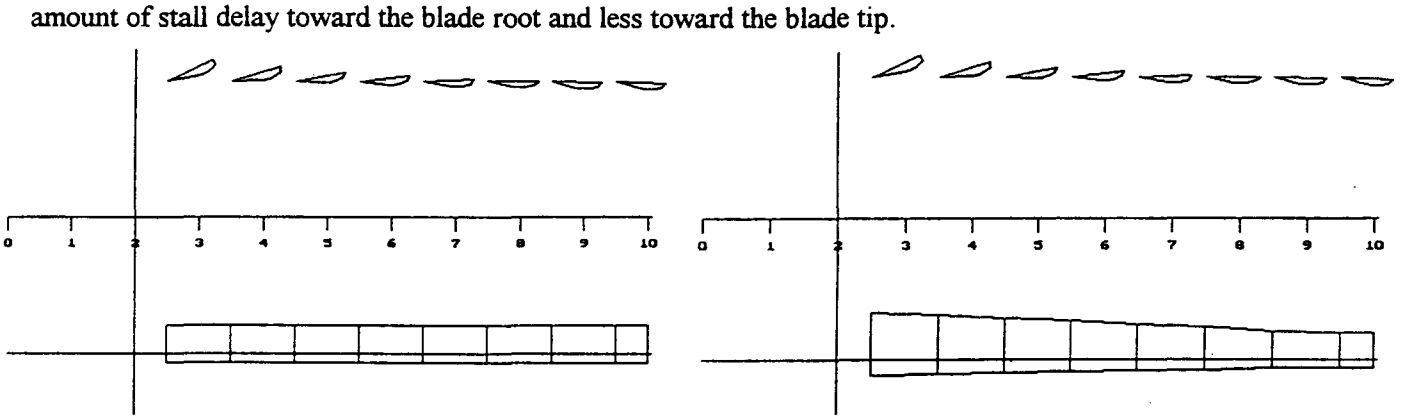

Fig. 3 Combined experiment blade geometries.

Table 1. Constant Chord and Tapered Chord Calculations of Stall-Delay Angle.

r/R CER	c/R	c/r	K	alfa clma	alfa clzer	del alfa	K*Θ/0.136	delay ang
0.050	0.050	1.000	0.178	9.000	-1.200	10.200	1.307	3.135
0.150	0.091	0.607	0.281	9.000	-1.200	10.200	1.254	2.588
0.250	0.091	0.364	0.448	9.000	-1.200	10.200	1.201	2.051
0.350	0.091	0.260	0.610	9.000	-1.200	10.200	1.168	1.709
0.450	0.091	0.202	0.768	9.000	-1.200	10.200	1.143	1.461
0.550	0.091	0.166	0.923	9.000	-1.200	10.200	1.124	1.266
0.650	0.091	0.140	1.076	9.000	-1.200	10.200	1.108	1.106
0.750	0.091	0.121	1.226	9.000	-1.200	10.200	1.095	0.971
0.850	0.091	0.107	1.375	9.000	-1.200	10.200	1.084	0.854
0.950	0.091	0.096	1.523	9.000	-1.200	10.200	1.074	0.751

r/R CER	c/R	c/r	K	alfa clma	alfa clzer	del alfa	K*Θ/0.136	delay ang
0.050	0.050	1.000	0.178	9.000	-1.200	10.200	1.307	3.135
0.150	0.157	1.043	0.171	9.000	-1.200	10.200	1.312	3.183
0.250	0.147	0.589	0.289	9.000	-1.200	10.200	1.250	2.555
0.350	0.138	0.394	0.418	9.000	-1.200	10.200	1.209	2.131
0.450	0.129	0.286	0.560	9.000	-1.200	10.200	1.177	1.802
0.550	0.119	0.217	0.722	9.000	-1.200	10.200	1.150	1.527
0.650	0.110	0.169	0.907	9.000	-1.200	10.200	1.126	1.285
0.750	0.100	0.134	1.122	9.000	-1.200	10.200	1.104	1.062
0.850	0.086	0.102	1.444	9.000	-1.200	10.200	1.079	0.805
0.950	0.082	0.088	1.681	9.000	-1.200	10.200	1.064	0.653

The baseline 2D wind-tunnel data set is shown in Fig. 4a for a Reynolds number of 1,000,000. Although a lower Reynolds number airfoil data set is desirable toward the blade root, this was the lowest Reynolds number data set acquired for the airfoil in the Delft wind tunnel. This data set provides good 2D stall characteristics for angles of attack up to 18 deg. The shape of the post-stall c_l distribution out to 18 deg is largely influenced by the forward movement of the upper surface separation point with increasing angles of attack. For simplicity, the stall delay c_l correction is introduced on the linear part of the lift curve slope that corresponds to 0.1, which is typically at an angle of attack of approximately 6 deg. This results in a 0.1 increase in c_l for each degree of stall delay as seen in Fig. 4b. Retaining the same 2D post-stall shape for the 3D post-stall distribution is questionable since it is strongly affected by the forward movement of the separation point on the blade. The forward movement of the separation point for 3D post-stall would likely differ from the 2D case. The significance of this difference needs further study. Beyond 18 deg the airfoil characteristics transition into flat plate theory.

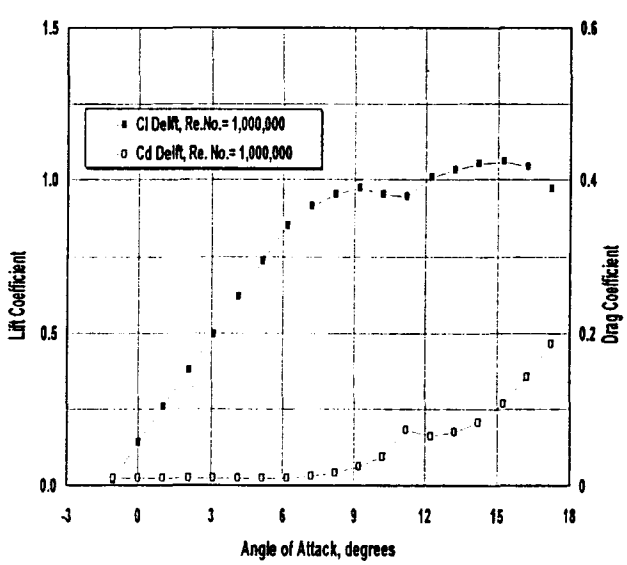

Fig. 4a S809 Delft 2-D wind tunnel data.

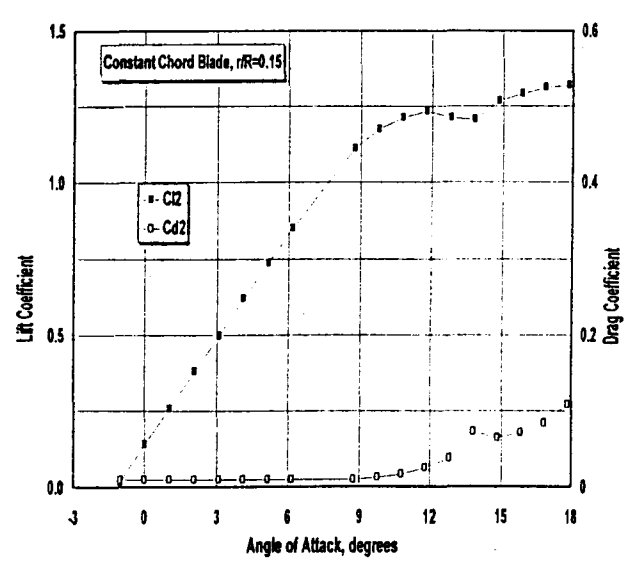

Fig. 4b S809 Delft data with stall delay.

For the constant-chord CER blade, the modified 2D data set, which includes the post-stall 3D lift and drag correction, is shown in Fig. 5a. All blade segment airfoil characteristics were modified to include 3D post-stall effects for the PROP93 performance prediction. For clarity, the airfoil characteristics are shown for only every other blade station. In the root region the post-stall $c_{l,max}$ increased from 1.1 to more than 1.3 as a result of 3 deg of stall delay. This increase in c_l is noticeably less than that observed on the CER for this radial station. Due to the blade's constant chord, which results in high tip region solidity relative to a tapered blade, noticeable stall delay of 0.75 deg is predicted for the tip region. Stall delay is also accompanied by a corresponding angle of attack delay for the exponential drag increase. This correction to the drag may not be appropriate as suggested by Harris.[12] In this regard, additional study is needed. For the tapered-chord blade, the modified 2D data set that includes a post-stall 3D lift and drag correction is shown in Fig. 5b.

For the CER, predicted rotor power was calculated using both 2D wind-tunnel data and modified data to account for 3D stall-delay effects. This was done for the current constant-chord/twisted blades and the hypothetical tapered-chord blade having the same chord at 80% radius, which results in a similar torque weighted equivalent chord. A comparison (Fig. 6a) of the predicted power curves for constant-chord/twisted blades showed a peak power increase of 23% for a 75% radius blade pitch of 11.5 deg toward feather which corresponds to a tip pitch of 8 deg for the test data. Although the constant chord blades have less inboard stall delay than a tapered blade they have more outboard stall delay. Slightly more stall delay in the tip region coupled with a high dynamic pressure helps to compensate for less stall delay inboard with a small dynamic pressure.

For the same peak power, the tapered/twisted blades required a pitch angle of 9 deg. A comparison (Fig. 6b) of the predicted power curves for the tapered/twisted blades showed a peak power increase of 28% which was slightly higher than the increase for the constant-chord/twisted blades. Generally, there was not a large difference in the peak power increase due to 3D stall delay for constant chord versus tapered blades.

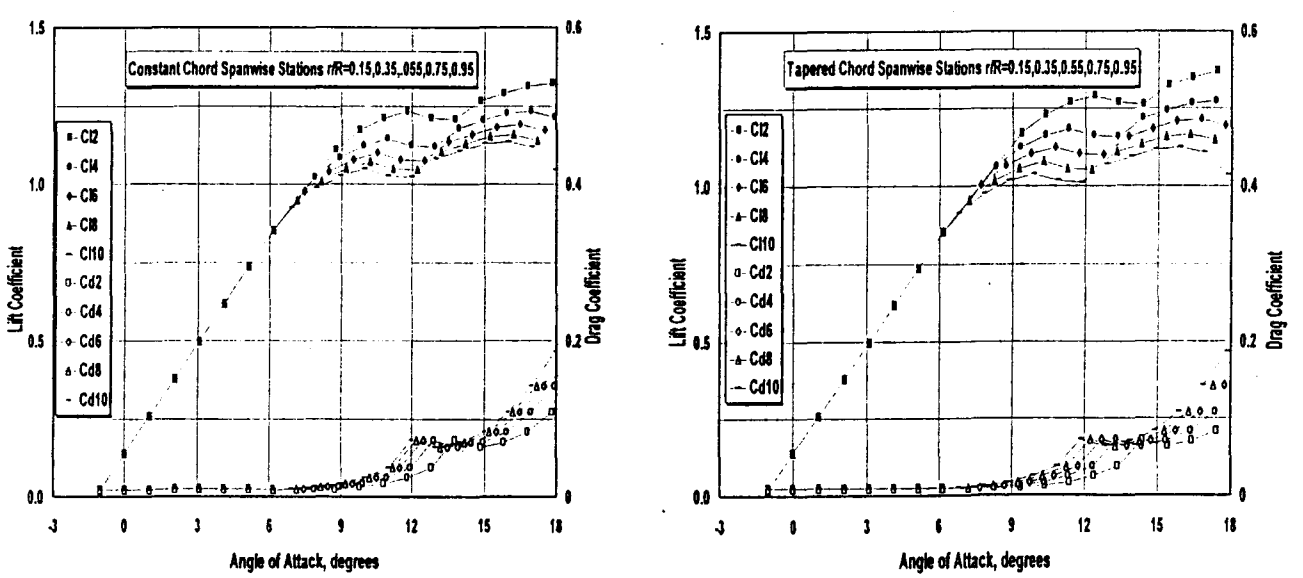

Fig. 5a & 5b Constant-chord and tapered-chord airfoil data sets modified to include post-stall 3D effects.

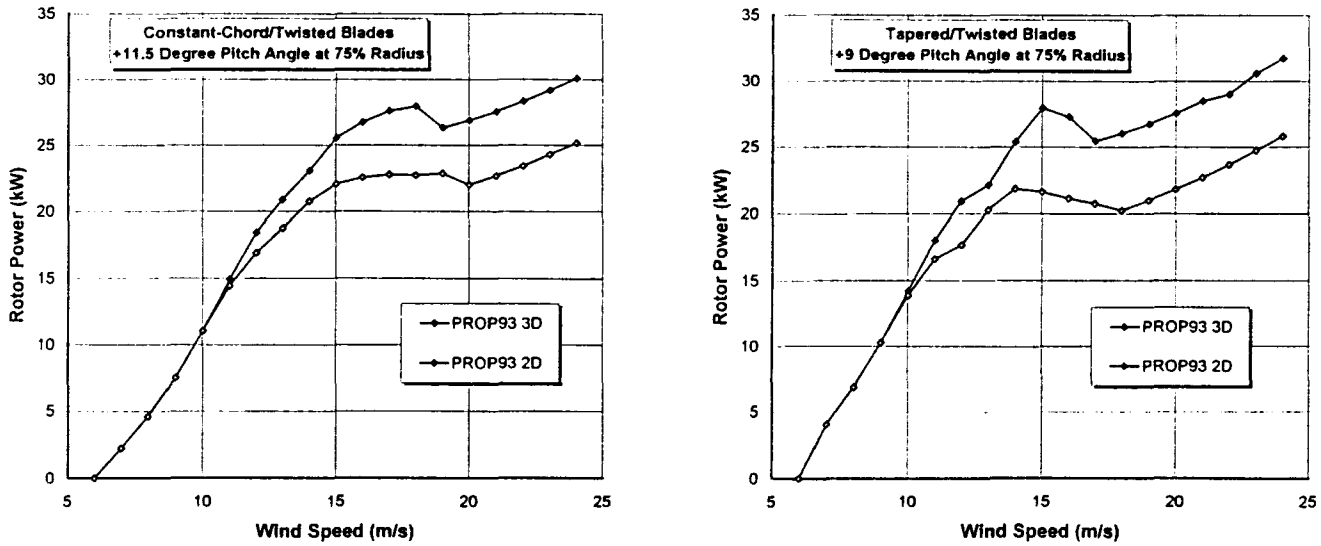

Fig. 6a & 6b Constant-chord and tapered-chord, blade predicted power for 2D and 3D airfoil characteristics.

AWT-26 Rotor

The low solidity AWT-26 blade shown in Fig. 7 was chosen as a representative, commercial blade to further evaluate the stall delay model. Application of the stall delay model to most commercial blades is more complex as a result of different airfoils from root to tip. The AWT-26 blade uses an NREL airfoil family that consists of three different airfoils[13] from blade root to tip. In the root region, a high $c_{l,max}$ S815 airfoil is used. This airfoil transitions into a thinner, lower $c_{l,max=1.0}$ S809 airfoil at 75% radius and then to a low $c_{l,max=0.9}$ S810 airfoil at 95% radius. For these airfoils, reasonably accurate 2D post-stall, wind-tunnel data is needed out to 20 degrees, which is not always available. Airfoil performance characteristics must then be predicted with the Eppler[14] code. With the airfoil's radial location and Reynolds number specified, input data sets can then be prepared using WTPREP.[15] This software package saves the designer much time since it interpolates between the different airfoil characteristics and Reynolds number for each of the spanwise segments as illustrated in Fig. 8a. Using the stall-delay model, the 2D data were modified to reflect 3.5 deg of stall delay in the root region that decreases to zero at the tip as seen in Fig. 8b. This results in a root region $c_{l,max}$ enhancement of 0.35 relative to 2D data. Predicted power using the 2D and modified 3D data sets is shown in Fig. 9. The data set with the 3D stall-delay resulted in a peak power increase of 18% relative to 2D data. Based on previous studies this percentage increase appears to be fairly realistic.

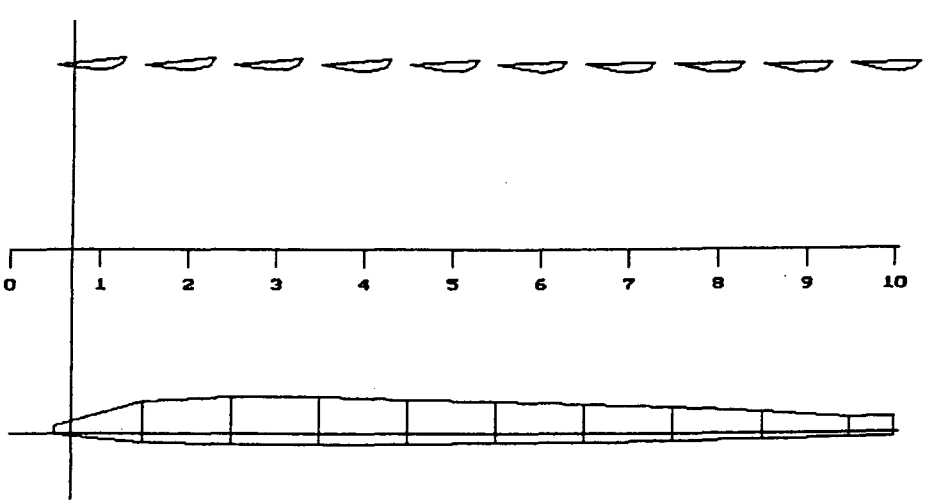

Fig. 7 AWT-26 blade geometry.

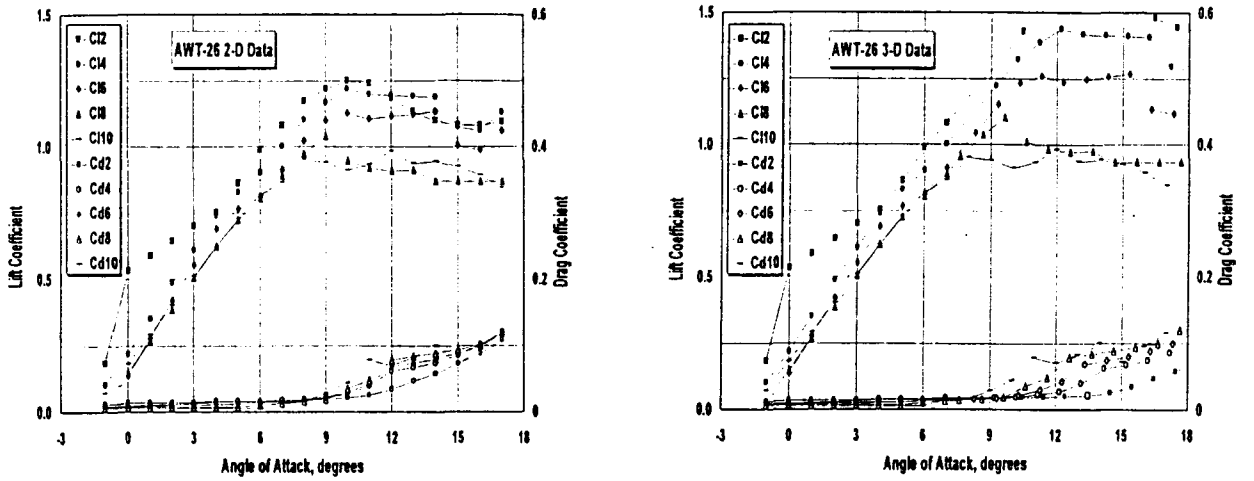

Fig. 8a & 8b S810, S809, and S815 airfoil 2D and 3D performance characteristics.

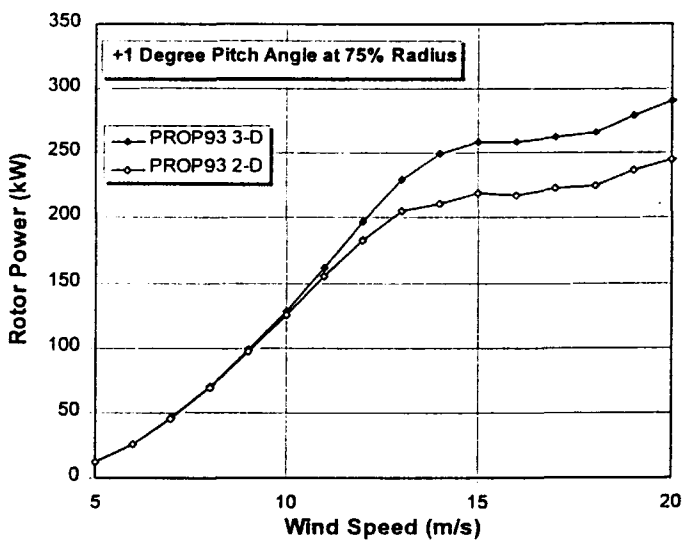

Fig. 9 AWT-26 rotor performance calculated with 2D data and the 3D post-stall model.

Comparisons of Measurements and Predictions

Comparisons between predicted and measured power for the CER and the AWT-26 showed discrepancies that raised questions, which could not be adequately answered. However, these discrepancies should not reflect on the accuracy of the Corrigan and Schillings stall-delay method.

Measured electrical power for the CER was obtained for a blade tip pitch angle of +8.0 deg. Each baseline cycle data point represents the power for one revolution in time. Relatively steady-state conditions were present for each data point where it differed little from adjacent cycles on each side of the data point. The yaw error for the data was limited to ±5 deg. These data sets were also binned on pitch angle since some elasticity in the control system resulted in a tendency for the pitch to shift about 1 1/2 deg toward feather at high wind speeds. To convert CER predicted rotor power into electrical power required the drive train efficiency curve of Fig. 10.

For the CER, good correlation with test data is shown in Fig. 11 at medium wind speeds. However, predicted peak power using the 3D stall delay correction was significantly higher than measured power while predicted peak power resulting from 2D post-stall characteristics was in closer agreement with test data. Potential error sources for the discrepancy with 3D post-stall calculations can be attributed to both power measurements and the inherent assumption that the shape of the 3D post-stall distribution is the same as the 2D post-stall distribution. It should be noted again, however, that the 3D post-stall model yielded a lower $c_{l,max}$ than experimental data. Another aspect to consider was that one of the three blades of the test rotor was covered with tuffs for flow visualization with a radially aligned video camera. Five large pressure probes were also mounted along the blade's leading edge. As a result, this blade had significantly more drag which likely accounts for a good portion of the discrepancy between 3D predicted and measured data. Further work is necessary to investigate these error sources along with the possibility that the empirical stall-delay model itself could be overestimating the lift enhancement.

Measured electrical power for the AWT-26 was obtained at the Tehachapi, California, wind site for a blade tip pitch of 1.0 deg.[16] The power curve was derived from 300 hrs of data using 1 min averages of 1 sec data points. While establishing this power curve, significant variations in turbine efficiency were noted with changes in the season and turbulence intensity. Predicted rotor power was converted into electrical power using the drive train efficiency curve of Fig. 12.

The comparison of predicted and measured power for the AWT-26 is shown in Fig. 13. The use of 2D airfoil data significantly underpredicts peak power. The use of the 3D-stall delay model provides better agreement with measured peak power but still underpredicts peak power by about 10%. Predicted power also includes a slight increase in rpm around peak power of 1.7% to account for generator slip. The discrepancy between predicted and measured power is partly related to lack of an adequate 2D-airfoil database and the omission of aerodynamic modeling of the tip brake plates. Typically, tip plates result in an increased angle of attack and power in the tip region. In addition, alterations of the measured power curve for seasonal and turbulence intensity has not been quantified.

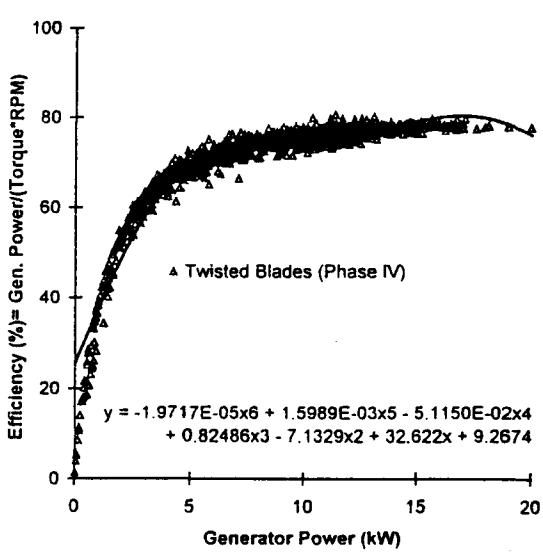

Fig. 10 Drive-train efficiency for the CER.

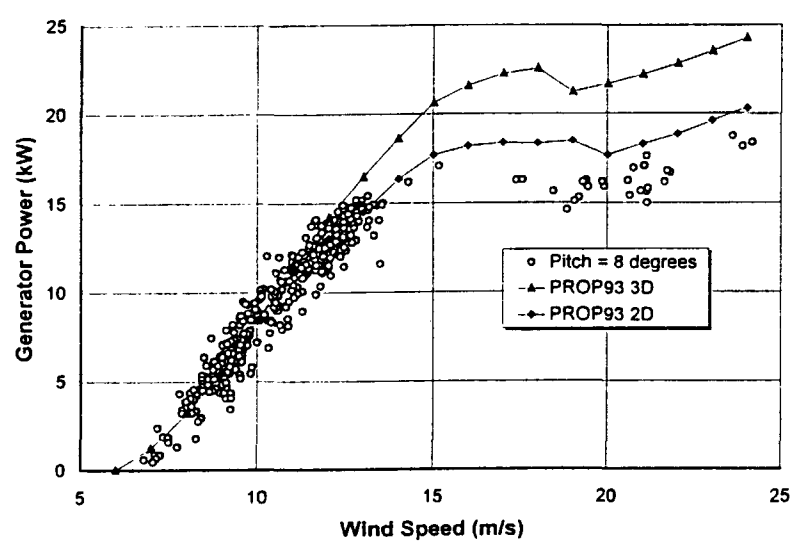

Fig. 11 Comparison of 2D and 3D predicted power curves with measured data for the CER.

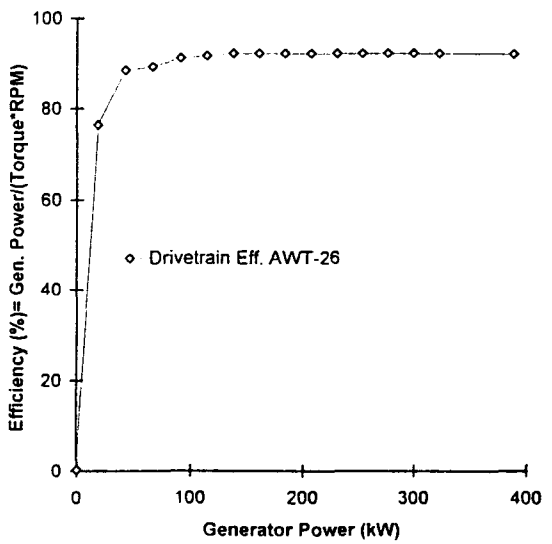

Fig. 12 Drive-train efficiency for the AWT-26.

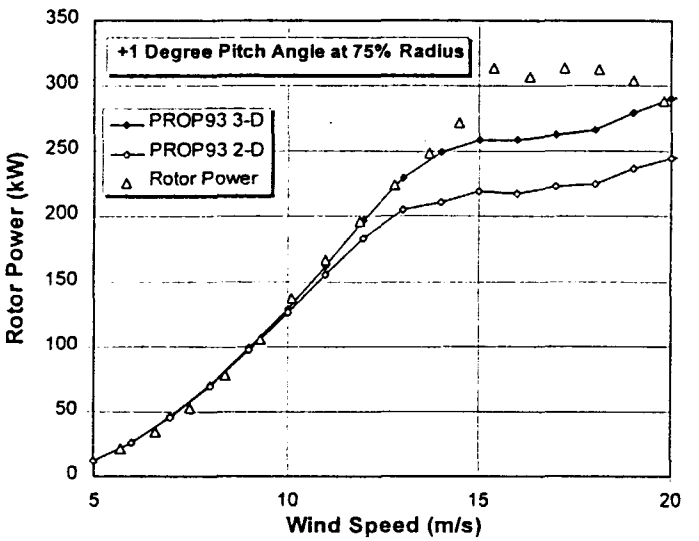

Fig. 13 Comparison of 2D and 3D predicted power curves with measured data for the AWT-26.

CONCLUSIONS

The Corrigan and Schillings empirical model for predicting stall delay due to rotation appears to quantify the first-order effects through the product of a shape factor that is proportional to the local blade solidity and the airfoil's angle of attack range for positive c_l which is proportional to its camber. The method is easy to implement by modifying the 2D airfoil data tables and provides a realistic increase in overall rotor power. The accuracy is dependent on the measured post-stall 2D airfoil characteristics up to large angles of attack of 18 deg and more. The method predicts a smaller increase in the root region c_l than CER data and inherently assumes that the 3D post-stall distribution will be similar to the 2D post-stall data, which is questionable.

Results of this investigation yielded peak power increases due to stall delay for the high solidity CER of 20% to 30% compared with results obtained from 2D data. For lower solidity, commercial rotors like the AWT-26, this increase was calculated to be 15% to 20%. Most of this gain is a result of extending the lift curve to greater values of c_l and up to 25% of the gain results from a wider drag bucket. Rotor power increase due to stall delay appears to be relatively insensitive to blade taper. The amount of stall delay increases for blade-pitch angles toward stall. Accounting for stall delay is most important for stall regulated rotors for accurately predicting peak power. Neglecting this 3D aerodynamic component leads to excessive blade solidity and peak power that has to be overcome by excessive blade pitch toward stall. The importance of including stall delay for variable pitch rotors and variable rpm is mainly for determining the wind speed for regulating peak power.

Recommendations for refining the prediction of stall delay should include the following work. A better understanding is needed of the influence of the blade's spanwise pressure gradient on stall delay. Also needed is an evaluation of the inherent assumption that the shape of the 3D post-stall c_l distribution is the same as that for 2D data. If the assumption is reasonable, the airfoil database for 2D post-stall needs to be extended for many airfoils to higher angles of attack. Correlation of the method with other rotor data sets is needed along with the evaluation of other post-stall models. Empirical constants used in the stall delay method require further evaluation for their reasonableness. Details of simplified empirical post-stall methods could also benefit from further comparisons with CFD predictions.

REFERENCES

[1]Himmelskamp, H., *Profile Investigations on a Rotating Airscrew*, MAP Volkenrode Reports and Translation No. 832, Sept. 1947.

[2]Ronsten, G., "Static Pressure Measurements on a Rotating and a Non-rotating 2.375 m Wind Turbine Blade. Comparison with 2D Calculations," European Wind Energy Conference, Amsterdam, 1991.

[3]Butterfield, C. P., Musial, W.P., Scott, G. N., and Simms, D. A., *NREL Combined Experiment Final Report - Phase II*, NREL/TP-442-4807, Golden, CO, Aug. 1992.

[4]Corrigan, J.J. and Schilling, J. J., "Empirical Model for Stall Delay Due to Rotation," American Helicopter Society Aeromechanics Specialists Conf., San Francisco, CA, Jan. 1994.

[5]Snel, H., Houwink, R., and Bosschers, J., " Sectional Prediction of Lift Coefficients on Rotating Wind Turbine Blades in Stall," ECN-C- -93-052, Dec. 1994.

[6]Banks, W., and Gadd, G., "Delayed Effect of Rotation on Laminar Separation," *AIAA Journal*, Vol. 1. (4) Apr. 1963.

[7]Sorensen, J. N., "Prediction of Three-Dimensional Stall on Wind Turbine Blade Using Three-Level, Viscous-Inviscid Interaction Model," European Wind Energy Conference, Italy, Oct. 1986.

[8]Narramore, J., and Vermeland, R., "Navier Stokes Calculations of Inboard Stall Delay Due to Rotation," *AIAA Journal of Aircraft*, Vol. 29 (12), Jan. 1992.

[9]Eggers, A. J., and Digumarthi, R. V., "Approximate Scaling of Rotational Effects on Mean Aerodynamic Moments and Power Generated by CER Blades Operating in Deep-Stalled Flow," 11th ASME Wind Energy Symposium, Houston, TX, Jan. 1992.

[10]Somers, D. M., *Design and Experimental Results for the S809 Airfoil*, NREL/SR-440-6918, Golden, CO, Jan 1997.

[11]McCarty, J., "PROP93 Interactive Performance Prediction Code with Graphics," Alternative Energy Institute, Canton, TX, 1993.

[12]Harris, F. D., "Preliminary Study of Radial Flow Effects on Rotor Blades," *Journal of the American Helicopter Society*, Vol. 11. (3), 1966.

[13]Tangler, J. L., and Somers, D. M., "NREL Airfoil Families for HAWTs," WindPower '95 Conference, AWEA, Washington D.C., Mar. 1995.

[14]Eppler, R., *Airfoil Design and Data*, Springer-Verlag, Berlin, 1990.

[15]Guglielmo, J. J., "An Airfoil Data Pre-Processing Code for Horizontal Axis Wind Turbines," DOE Wind Program Subcontractor Review Meeting, Denver, CO, Aug. 1995.

[16]Griffin D. A., "AWT Experience with PROP Modeling," 10th IEA Symposium on Aerodynamics of Wind Turbines, Edinburgh, Dec. 1996.